

Article

Soil Erosion Assessment Using the RUSLE Model, Remote Sensing, and GIS in the Shatt Al-Arab Basin (Iraq-Iran)

Hadi Allafta *  and Christian Opp 

Faculty of Geography, Philipps-University of Marburg, Deutschhausstr. 10, 35037 Marburg, Germany

* Correspondence: allafta@students.uni-marburg.de

Abstract: In the Shatt Al-Arab basin, soil erosion is a major problem due to the steepness of the terrain and the significant difference in altitude between the upstream and downstream parts of the basin. Vast quantities of soil are moved annually, resulting in massive repercussions including soil degradation, structural damage, biodiversity loss, and productivity reduction in the catchment area, huge sediment load, and the pollution of streams and rivers. Consequently, the assessment of soil erosion risk and geographical distribution is essential for constructing a database for developing effective control strategies. Revised Universal Soil Loss Equation (RUSLE) was combined with Remote Sensing (RS) and Geographic Information System (GIS) in the current work to define the soil erosion hazard map in the Shatt Al-Arab basin. The RUSLE model included various characteristics for soil erosion zonation including rainfall erosivity, soil erodibility, slope length and steepness, land cover and management, and conservation support practices. Annual erosion rates in this study in tons per hectare were: extremely high (more than 50); very high (50 to 16.5); high (16.5 to 2.2); medium (2.2 to 1); and low (1 to 0) $\text{ton ha}^{-1}\text{year}^{-1}$ representing 16, 4, 13, 7, and 60 % of the basin's area, respectively. The high soil loss rates are associated with heavy rainfall, loamy soil predominance, elevated terrains/plateau borders with a steep side slope, and intensive farming. Managers and policymakers may use the results of this study to implement adequate conservation programs to prevent soil erosion or recommend soil conservation acts if development projects are to proceed in places with a high soil erosion risk.

Keywords: geographic information system; remote sensing; revised universal soil loss equation; Shatt Al-Arab basin; soil erosion



Citation: Allafta, H.; Opp, C. Soil Erosion Assessment Using the RUSLE Model, Remote Sensing, and GIS in the Shatt Al-Arab Basin (Iraq-Iran). *Appl. Sci.* **2022**, *12*, 7776. <https://doi.org/10.3390/app12157776>

Academic Editor: Itzhak Katra

Received: 4 July 2022

Accepted: 31 July 2022

Published: 2 August 2022

Publisher's Note: MDPI stays neutral with regard to jurisdictional claims in published maps and institutional affiliations.



Copyright: © 2022 by the authors. Licensee MDPI, Basel, Switzerland. This article is an open access article distributed under the terms and conditions of the Creative Commons Attribution (CC BY) license (<https://creativecommons.org/licenses/by/4.0/>).

1. Introduction

Human requirements in the twenty-first century, such as foods, fibers, clean water, and clean air, cannot be met without healthy soil [1]. Soils are an essential component of earth system functions that facilitate the supply of essential ecosystem services [2,3]; however, the soil may be degraded by human activities and environmental stressors [4]. Population increase, deforestation, and overgrazing are the three major factors that cause and exacerbate soil erosion [5]. Erosion has many negative effects that are of real concern for a variety of reasons. Firstly, removal of the fertile top layer of soil (topsoil) by erosion affects soil fertility and crop productivity. Secondly, erosion diminishes reservoir capacity and operation and degrades downstream water quality [6–8]. Thirdly, soil erosion causes a rise in pollutants and sedimentation in streams and rivers, resulting in the blockage of these waterways as well as a reduction in biodiversity [9]. Fourthly, erosion also transports soil-laden water downstream, which may produce sediment layers that impede the flow of streams and rivers and ultimately cause floods [10]. Lastly, erosion destroys the land that can host fewer plants capable of absorbing climate-warming carbon dioxide. In a given year, soils might theoretically store enough greenhouse gases (GHG) to equal around five percent of all human-made GHG emissions [11]. An approximate estimate indicates that 10 million hectares of croplands are ruined annually owing to soil erosion.

Due to this, agricultural output decreases, resulting in declining economies and a rise in malnutrition [12].

In the Shatt Al-Arab basin, a trans-boundary basin between Iraq and Iran, soil erosion is a severe and complicated environmental problem [13,14]. The soil erosion rates in Iran, where most of the basin is situated, are twenty times the world average. Soil erosion treatment costs Iran between USD 56B and USD 112B, which is more than the nation's annual oil earnings (e.g., USD 53.6B in 2014) [15]. Moreover, degraded areas are often less capable of retaining water, which may exacerbate floods. For instance, massive flash floods in the Shatt Al-Arab basin in 2019 [16] destroyed livelihoods and caused billions of dollars in damage in Iraq and Iran [17,18]. In the region of Khuzestan, where the Shatt Al-Arab basin extends, roughly 18 tons of soil per hectare is eroded each year [19]. Khuzestan province ranks first in Iran due to the high soil erosion rates. Such high erosion levels restrict the viability of agricultural endeavors [20]. In other instances, soil erosion has led to an increase in dust pollution in this area, which has harmed the habitability of rural households [21–23]. Moreover, sedimentation caused by erosion affects the storage capacity of dams by about 0.2 billion cubic meters each year. Likewise, Iran's agricultural land losses are around 33-ton ha⁻¹year⁻¹ of soil due to erosion. A ton of soil encloses around 28 kg of nitrogen, phosphorus, and potassium. Consequently, approximately 900 kg of nutrients per hectare are lost [24]. Based on the average cost of fertilizers, the annual damage of nutrient loss due to soil erosion is around USD 2.7B [25]. The above-described erosional degradation results in enormous economic impacts in the upper parts of the basin. Moreover, the downstream parts of the basin have a limited potential for soil erosion. Yet, materials that are eroded from the upstream parts may compile in the river's lower reaches, imposing further economic damages [14]. Studies conducted on soil erosion in the Shatt Al-Arab basin were limited to the Iranian part of the basin, e.g., [26,27]. Such studies were valuable in their own terms. However, they were constrained to specific sites within the basin. Therefore, it is not possible to thoroughly identify the spatial distribution characteristics of the soil erosion in the entire basin. From this perspective, we think that erosion hazard assessment may help both riparian countries, since there is a high likelihood that their citizens and leaders will come to a consensus on the need for collaboration, e.g., [28]. Initiatives and sustainable development programs must be carried out on a realistic geographical scale that enables the full expression of hydrologic interrelationship between all the components of a landscape continuum. In this case, the appropriate scale is the full Shatt Al-Arab river basin.

Soil erosion hazard assessment has been used by scientists since the 1930s [29,30] to forecast and detect control erosion techniques. Various methodologies have been used to estimate soil loss by water at various levels including global, regional, and local [28–34]. Several models have been created to assess soil loss rates [12,35]. These models are divided into three types: physical-process-based models, empirical models, and semi-empirical models [36]. Field-based models for quantifying soil loss and its spatial variety are expensive and time-consuming, and insufficient sample plots might impair the consistency of the actual spatial degree of the areas experiencing erosion. In the outdated field-based methods, carefully mapping and monitoring the spatial distribution of soil loss in extremely wide zones is an arduous, expensive, and time-consuming task [37]. On the other hand, each regional scale erosion model such as USLE/RUSLE, SEMMED, WEPP, ANSWERS, EUROSEM, LISEM, SWAT, AGNPS, and SWRRB has its unique features and range of application [38–45]. The Universal Soil Loss Equation (USLE) was established by the Department of Agriculture in the United States in 1978 to forecast the amount of eroded soil over time [46]. It is an empirical technique that evaluates the long-term means of rill and sheet erosion based on plot data collected in the eastern United States [47]. The authors of [48] provided a newer version of USLE called the Revised Universal Soil Loss Equation (RUSLE). Despite being an empirical method, the combination of RS, GIS, and RUSLE produces soil erosion estimates and its geographic distribution at acceptable costs and with greater precision across larger regions [49–54]. The authors of [40,53,55] observed that the

empirical equation of RUSLE remains the most suitable method for assessing soil erosion risk owing to its low data requirements and easy model structure. This is particularly true for most developing nations, where the application of more complicated models may be constrained by a lack of acceptable input data [36]. Therefore, this study aimed to assess soil loss in the Shatt Al-Arab basin using RS, GIS, and the RUSLE model. This may be used by decision-makers for optimal soil restoration planning and sustainable land management practices.

2. Study Area

The Shatt Al-Arab basin consists of the Tigris and Euphrates basins, as well as the Karun and Karkheh sub-basins (Figure 1). The Shatt Al-Arab, which begins at the confluence of the Tigris and Euphrates rivers near Qurna city, flows for about 100 km to the south before forming the boundary between Iran and Iraq for the last 90 km of the route, before emptying into the Gulf. The entire area draining to the river, excluding the Tigris and Euphrates basins but including the Karun and Karkheh sub-basins, is around 143,000 km². The Karun River, a tributary of the Shatt Al-Arab, flows wholly across Iranian territories between 30° and 34° N and 48° and 52° E. The Karun watershed elevations range from 0 to 4400 m above sea level with annual precipitation ranging from 50 to 1800 mm [56]. The river is 950 km long and has an average discharge of 575 m³/s. The river's path to the Gulf splits into two main branches: Bahmanshir and Haffar, which join the Shatt Al-Arab. It stems from the Zagros Mountains near Zard-Kuh in western Iran. The watershed consists mainly of elongated piedmont fan and valley terrace deposits [57]. The Karkheh River is situated in Iran's southwest region between 30° and 35° N and 46° E to 49° E. It is one of the most productive watersheds in Iran, accounting for 9% of the country's total irrigated land. In addition, the basin produces 10–11 percent of the country's wheat [58]. The watershed's elevation varies from less than 10 m above sea level in the south to more than 3500 m in the north. The southern part of the watershed receives roughly 150 mm of annual precipitation, whereas the northern part receives up to 750 mm [59]. The watershed situated in the Zagros Mountains is underlain by Phanerozoic sedimentary sequences that have resulted in the formation of hundreds of anticlines and synclines. The lithology in the basin is classified based on resistance as low (alluvial deposits, marl, and conglomerate); intermediate (gypsum, dolomitic limestone, and gypsums marl); and high (limestone and sandstone) [60,61].

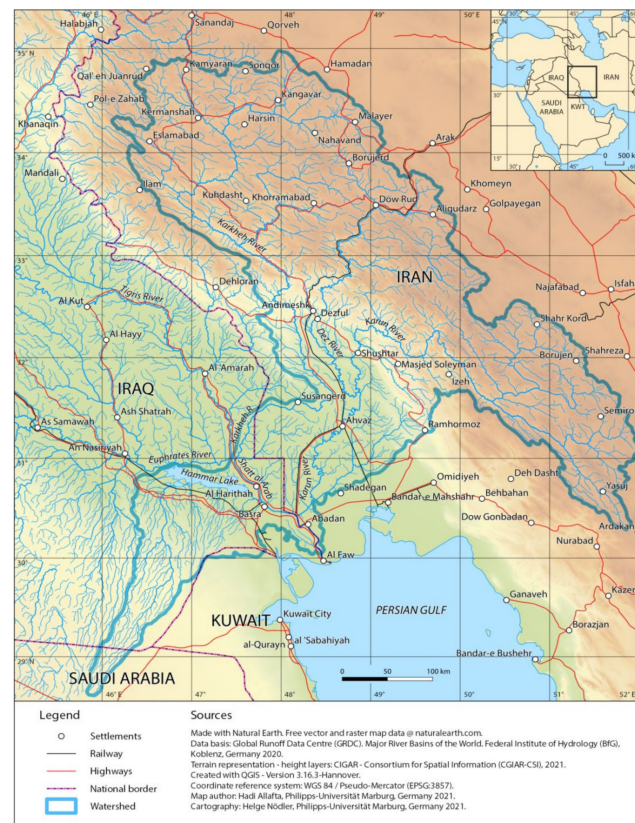


Figure 1. Study site. Note. From “GIS-based Multi-Criteria Analysis for Flood Prone Areas Mapping in the Trans-boundary Shatt Al-Arab Basin, Iraq–Iran” [62].

3. Methodology

Soil erosion, the most significant land degradation activity in the Shatt Al-Arab basin, is described as a leveling action in which soil and rock fragments are transported downslope by gravity. The RUSLE, a predictive empirical model, is used in the present study to calculate the annual soil loss in the Shatt Al-Arab basin. The RUSLE is the most extensively used erosion method to forecast the average annual soil loss through computing the soil erosion parameters [48]. It is a refined form of the USLE model [63], which has been thoroughly examined and applied for decades. The RUSLE calculates the average annual soil loss in tons per hectare based on five parameters:

$$A = R \times K \times LS \times C \times P \quad (1)$$

where A represents the average annual soil loss ($\text{ton ha}^{-1} \text{year}^{-1}$); R denotes the rainfall erosivity parameter ($\text{MJ mm ha}^{-1} \text{h}^{-1} \text{year}^{-1}$); K represents the soil erodibility parameter ($\text{ton h MJ}^{-1} \text{mm}^{-1}$); L denotes the slope length parameter; S refers to the slope steepness parameter; C represents the cover and management parameter; and P denotes the conservation support practices parameter. The LS, C, and P are dimensionless parameters [64]. After calculating the RUSLE parameters and preparing a raster format for each parameter, the soil erosion map was prepared by using “Raster Calculator”, which is a tool under “Spatial Analyst Tools” in ArcGIS. The erosion rate of a region pertains to an interaction between climate, topography, soil, and land use (Figure 2). The RUSLE model of predicting soil erosion in the Shatt Al-Arab basin was performed by incorporating all the factors that determine the erosion rates ($\text{ton ha}^{-1} \text{year}^{-1}$).

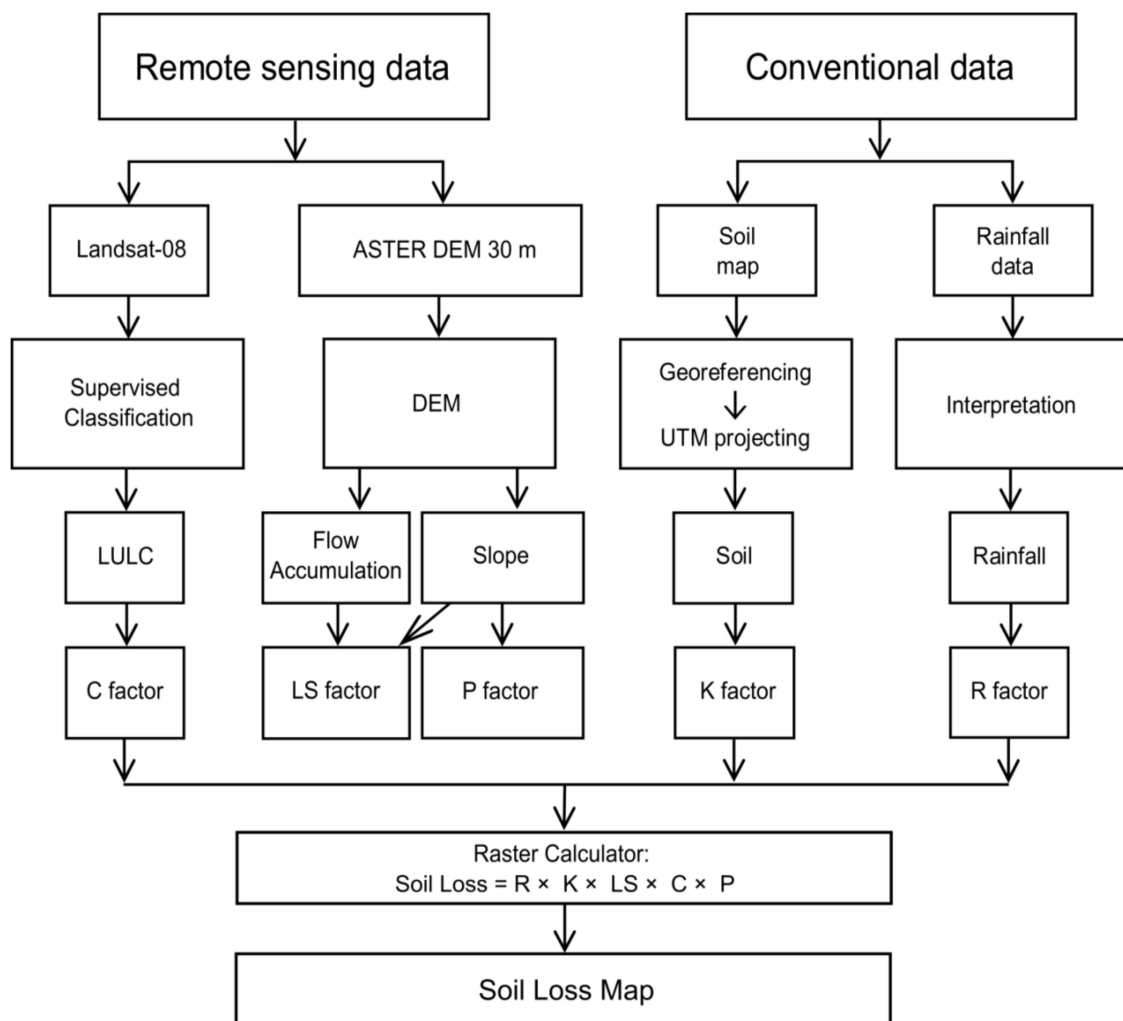


Figure 2. Flowchart of data processing for RUSLE model.

3.1. Rainfall Erosivity Factor (R Factor)

Rainfall erosivity (R) is a function of rainfall's ability to cause soil erosion by separating and moving soil particles. R calculation necessitates continual and thorough rainfall data [65]. R-factor computation is a complicated process that is highly dependent on the duration, amount, intensity, energy, and size of raindrops, as well as on precipitation pattern and subsequent runoff rates [66]. The rainfall intensity can be used to calculate rainfall erodibility [48,67]. However, determining the R-factor is a challenging task in most parts of the world due to the scarcity of high-resolution rainfall data [68]. Several studies conducted in Iran in sub-catchments within the Shatt Al-Arab basin used monthly and annual precipitation data, e.g., [26,27,69]. However, due to the lack of monthly precipitation data across the entire basin, we used an equation by [70] that required only annual precipitation data. This equation profitably generated compatible R results with the equation applied in the aforementioned studies, i.e., [26,27,69].

$$R = 79 + 0.363 \times X_a \quad (2)$$

where X_a is the mean annual precipitation. The Climate Research Unit data (www.cru.uea.ac.uk/data accessed on 9 November 2020) was used to retrieve the annual precipitation of the study region from 2011 to 2018. We transformed the precipitation data to a raster layer in ArcGIS 10.4.1 using "Multidimensional Tools" and "Make NetCDF Raster Layer". Using "Conversion Tools", the raster layer was then converted to points. Finally, we used

“Kriging”, a tool in “Spatial Analyst Tools”, to build the basin rainfall map using the acquired points [62].

3.2. Soil Erodibility Factor (K Factor)

Soil erodibility represents the intrinsic resistance of soil to erosion by rain and runoff, and it is a reflection of the interactions of physical and chemical features of soil that influence detachment, transportation, and infiltration capacity. The soil’s texture, structure, organic matter content, permeability, and its iron, aluminum, and salt concentration are among the most important determinants of erodibility [71]. The soil map of the basin was derived from the Geo Network Web Portal for Food and Agriculture Organization (FAO) Soil Map [72]. In addition, the SWAT Soil archive [73] was queried for soil types. The soils in the research region were categorized into seven textural categories, and the appropriate K value was determined using the table published by [74] (Table 1). The texture is a function of a soil’s grain size distribution.

Table 1. Soil features and the corresponding K factor.

Textural Class	K Factor (ton/Hectare)
Clay	0.49
Clay loam	0.60
Loam	0.67
Loamy sand	0.09
Sand	0.04
Sandy clay	0.45
Silty clay	0.58

3.3. Slope Length (L) and Slope Steepness (S) Factor (LS Factor)

The LS factor describes the impact of topography on erosion, which is directly proportionate to the slope’s length and gradient. The LS factor map was generated using the Digital Elevation Model (DEM) in the ArcGIS environment [6]. The terrain effects on erosion are assessed using the LS parameter, which is the product of slope length (L) and slope steepness (slope angle) (S). The escalating runoff accumulation towards the downslope increases the total soil erosion as the slope length (L) increases. Similarly, as the slope steepness rises, the runoff velocity and erosivity rise consequently [75,76]. Using ArcInfo, an ArcGIS Spatial analyst extension, the combined LS factor was calculated. The authors of [77,78] proposed the following equation, which was applied to a 30 m DEM cell size in the present study:

$$LS = (\text{Flow Accumulation} \times \text{Cell size} \div 22.13)^{0.4} \times (\sin \text{ slope} \div 0.896)^{1.3} \quad (3)$$

where LS equals the merged slope length and slope gradient factors; flow accumulation represents the cumulative upslope contributing region for a particular cell; cell size equals the size of the grid cell; and sine slope equals the sin of the slope angle in degrees. We used ArcGIS Spatial Analyst Plus together with the Arc hydro extension to estimate the flow accumulation and slope steepness from the DEM. The DEM data were retrieved from EARTHDATA Search [79] by defining the basin through the Advanced Spaceborne Thermal Emission and Reflection Radiometer (ASTER) DEM V003. Images of 30 m resolution were then downloaded from ASTER-DEM. We imported these images into

ArcGIS and mosaicked them using “Mosaic to New Raster”, a tool in “Data Management Tools”. After identifying the Universal Transverse Mercator (UTM) zone, the merged map was re-projected. Then, we applied “Fill Sinks” from Arc Hydro Tools > Terrain Processing > DEM Manipulation. Next, we selected “Flow Direction” and “Flow Accumulation” from “Terrain Processing” to obtain the flow accumulation. The slope was generated using the ArcGIS 10.4.1 tools Spatial Analyst Tools > Surface > Slope.

3.4. Cover and Management (C Factor)

The C factor describes how LULC types affect the soil loss rate [48]. Calculating the C factor values within the RUSLE method necessitates information regarding the soil management condition, the function of crops and canopies residues as a soil cover, soil moisture condition, and soil surface unevenness. However, evaluating any of these parameters is challenging due to many potential combinations and the paucity of data [66]. In accordance with [80–82], we used LULC classification for C factor determination in this study. The basin was classified into the appropriate LULC categories, and the C parameter was derived from the basin's LULC map. Then, we converted the raster map to vector format to provide the equivalent C factor for each LULC type based upon a literature recommendation from [83] (Table 2).

Table 2. The C factor for different land use land cover (LULC) classes.

LULC	C Factor Range	Mean
Shrubland	0.01–0.02	0.015
Urban	0.05–0.1	0.075
Crops	0.3–1	0.65
Barren	0.4–0.6	0.5
Water/Wetland	0	0

We retrieved the LULC data from Earth Explorer's land cover data [84]. The acquired images were imported into ERDAS IMAGINE 2014 for enhancement and processing. In ERDAS IMAGINE, we categorized the LULC using the supervised method. In the supervised method, polygons are selected, digitized, and placed in an "Area of Interest" layer to generate signature files. Multiple polygons were produced for a certain LULC class to give it a distinct class. The supervised categorization method is time-consuming, but it yields more overall accurate results than the unsupervised categorization method [85].

3.5. Conservation Support Practice Factor (P Factor)

The P factor quantifies the influence of conservation strategies, such as buffer belts of close-growing plants, contouring, and terracing on soil loss at a specific site. Adopting these supportive conservation practices reduces the P-value because they limit runoff volume and velocity and promote sediment deposition on the slope surface. In the literature, several tables and equations suggesting P values for the various supportive conservation actions have been documented [86–89]. In this study, the Wener approach [90,91] was used to compute the P factor, using the following formula:

$$P = 0.2 + 0.03 \times S \quad (4)$$

where S denotes the slope grade (%).

4. Results and Discussion

4.1. Rainfall Erosivity Factor (R-Factor)

The average annual rainfall data were used to compute the rainfall erosivity (R factor). The latter varied from 79.36 to > 80.81 MJ mm ha⁻¹ h⁻¹ year⁻¹. The prevailing pattern of the average annual rainfall in the study area displays the highest values in the northern portions and exhibits a southwards gradient towards the Gulf. Therefore, a high R factor is anticipated in the northern parts of the study area as R increases in such parts, while it decreases in the south (Figure 3). Specifically, the R factor of the study area has five classes: 79.36 to 79.73; 79.73 to 80.09; 80.09 to 80.45; 80.45 to 80.81; and >80.81 MJ mm ha⁻¹ h⁻¹ year⁻¹ representing 23.5, 20.3, 11.8, 23.0, and 21.4% of the basin area, respectively.

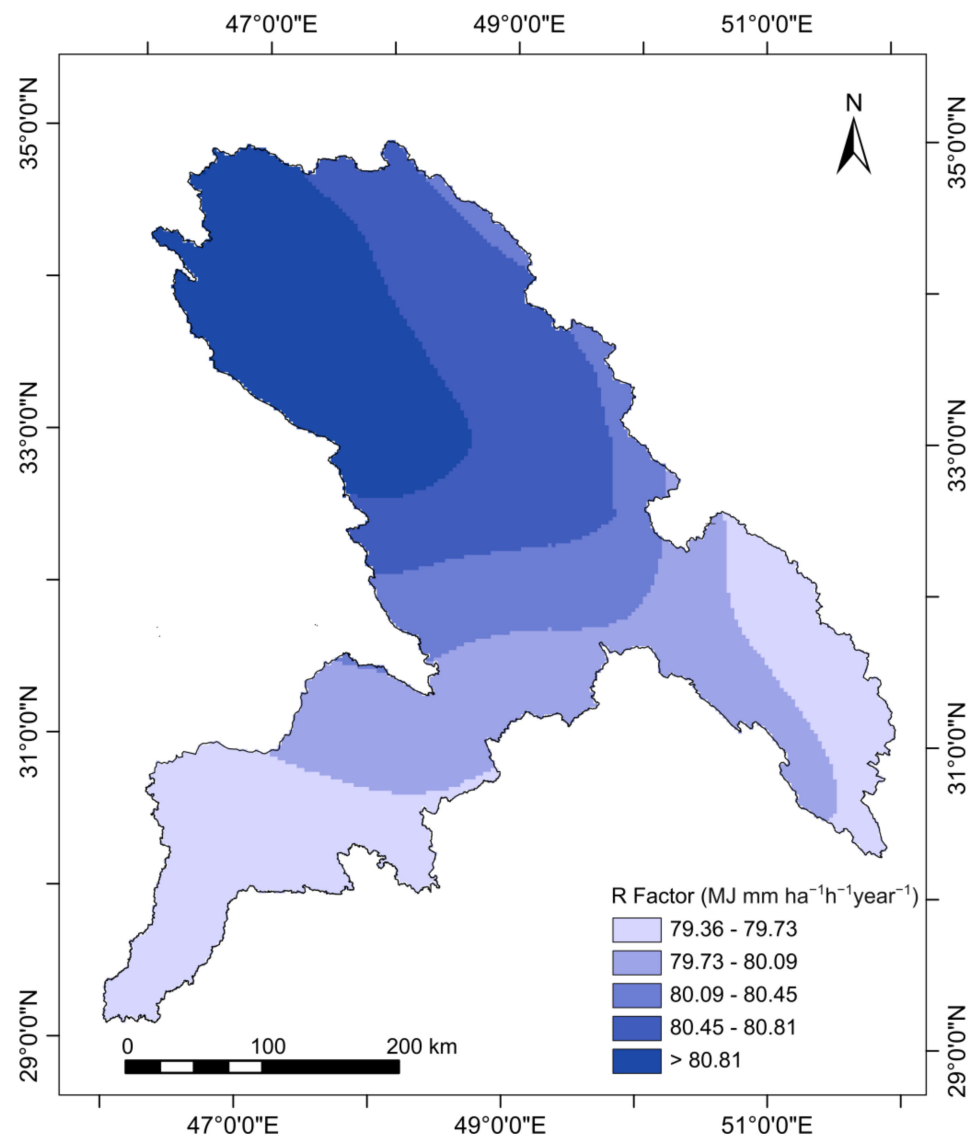


Figure 3. Spatial distribution of R factor in the study area.

4.2. Soil Erodibility Factor (K Factor)

Clay-rich soils have low K values due to their resistance to separation. Coarse-grained soils, such as sandy soil, have a low K level due to their low runoff potential, although being readily disintegrated. Medium-grained soils, such as loamy soils, have high K levels as they are more prone to disintegration and generate more runoff [64,92]. The research area's K factor is divided into five categories. These categories are 0.67, 0.58, 0.45, 0.09, and 0.04 $\text{ton h MJ}^{-1} \text{mm}^{-1}$ occupying 90.9, 0.6, 1.7, 5.3, and 1.6 of the basin's area, respectively (Figure 4) The K factor was high in most parts of the basin where loamy soils were dominant (light blue color in the figure represents loam and clay loam soils). On the other hand, sandy and clayey soils that constitute only around 10 percent of the basin's area exhibit low erodibility (green and red colors represent sand and loamy sand soils, respectively, while blue and yellow colors represent sandy clay and silty clay soils, respectively).

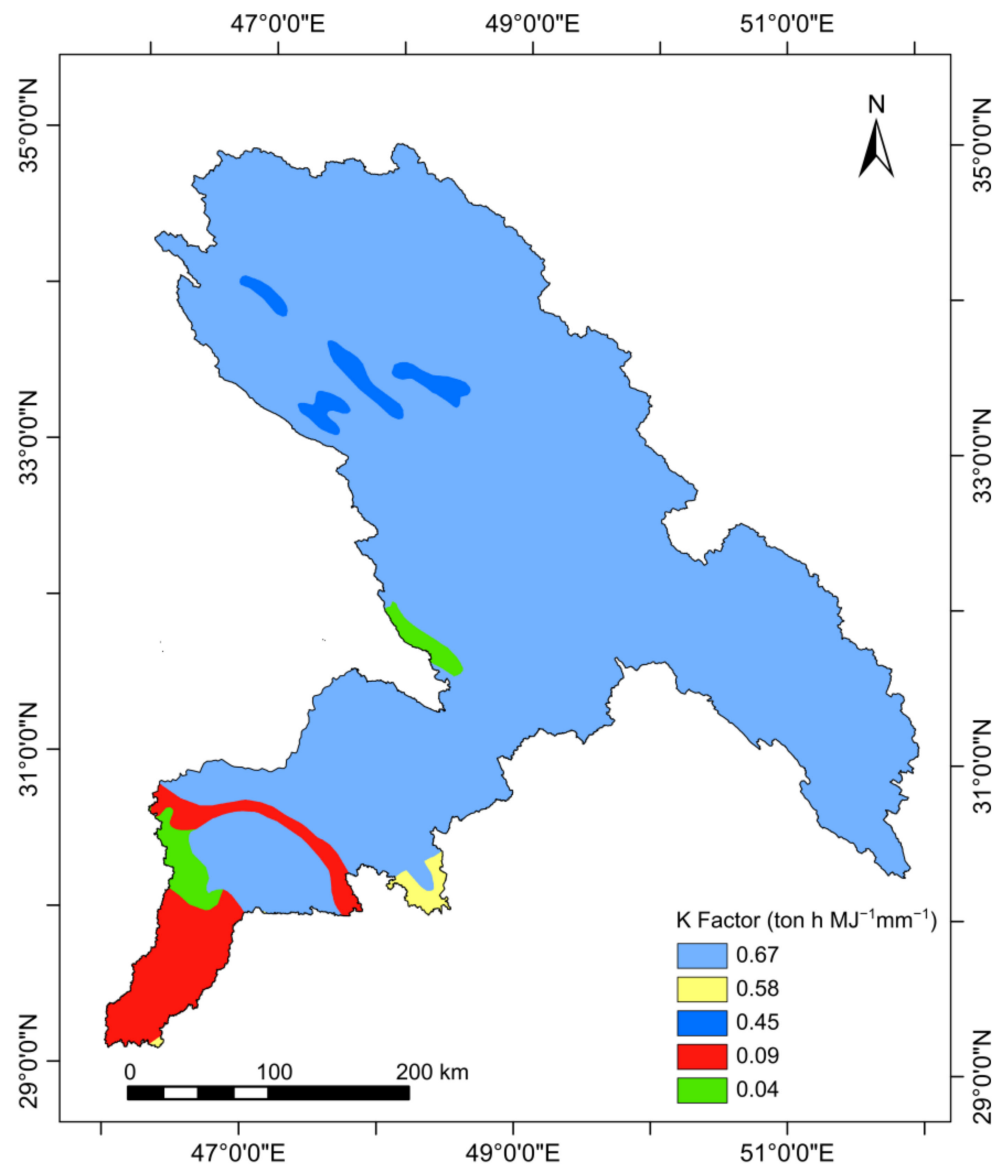


Figure 4. Spatial distribution of K factor in the study area.

4.3. Slope Length (L) and Slope Steepness (S) (LS Factor)

The LS factor was calculated by considering the slope and flow accumulation as inputs, although it depends on slope more than on flow accumulation (Equation (3)). The lowest LS values occupy the low-lying southern lands, reflecting the slope effect on the LS outcomes. In contrast, the highest LS values are situated in the complex northern and eastern landforms of the study area with steep slopes [61] between the anticlines and synclines (Figure 5). The LS factor of the basin has five classes: 0 to 2; 2 to 10; 10 to 25; 25 to 50; and >50, representing 63.2, 21.2, 11.8, 2.9, and 0.9% of the basin's area, respectively.

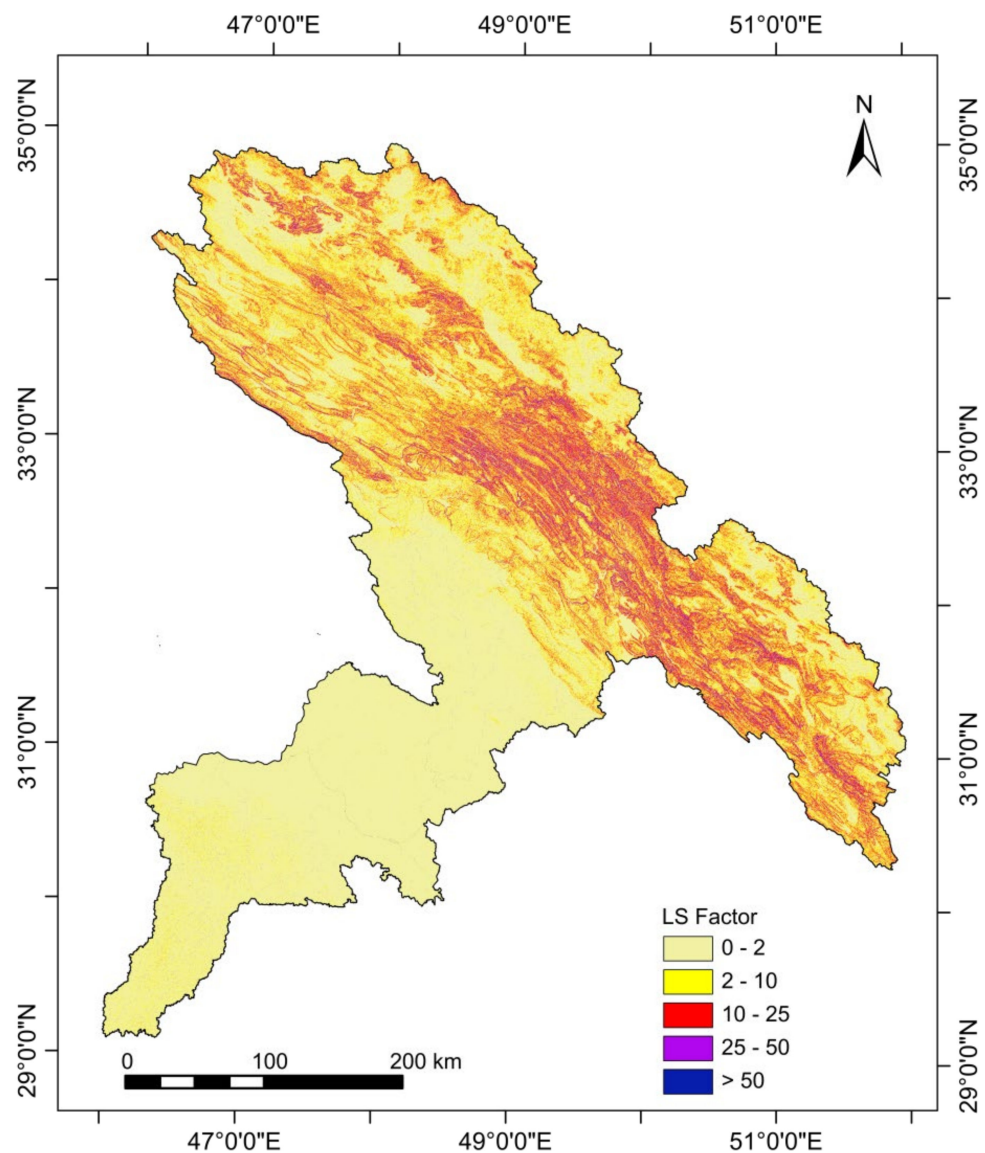


Figure 5. Spatial distribution of LS factor in the study area.

4.4. Cover and Management Factor (C Factor)

The study area's primary land-use types are barren, cropland, and shrub land. Water/wetland and urban land use represent a small ratio of the land use categories in the basin. Based on the existing literature, the C factor values assigned to each LULC category were 0.5, 0.015, 0.65, 0.075, and 0 for bare land, shrub land, cropland, urban, and water/wetland, respectively (Figure 6). Cropland that prevails in the northern and middle parts of the basin has the highest C factor (i.e., 0.65). Likewise, bare land that extends over the southwestern parts of the study area has a high C factor (i.e., 0.50). Cropland, bare land, urban, shrub land, and water/wetland occupy 12.7, 50.5, 0.9, 35.1, and 0.7% of the basin's area, respectively.

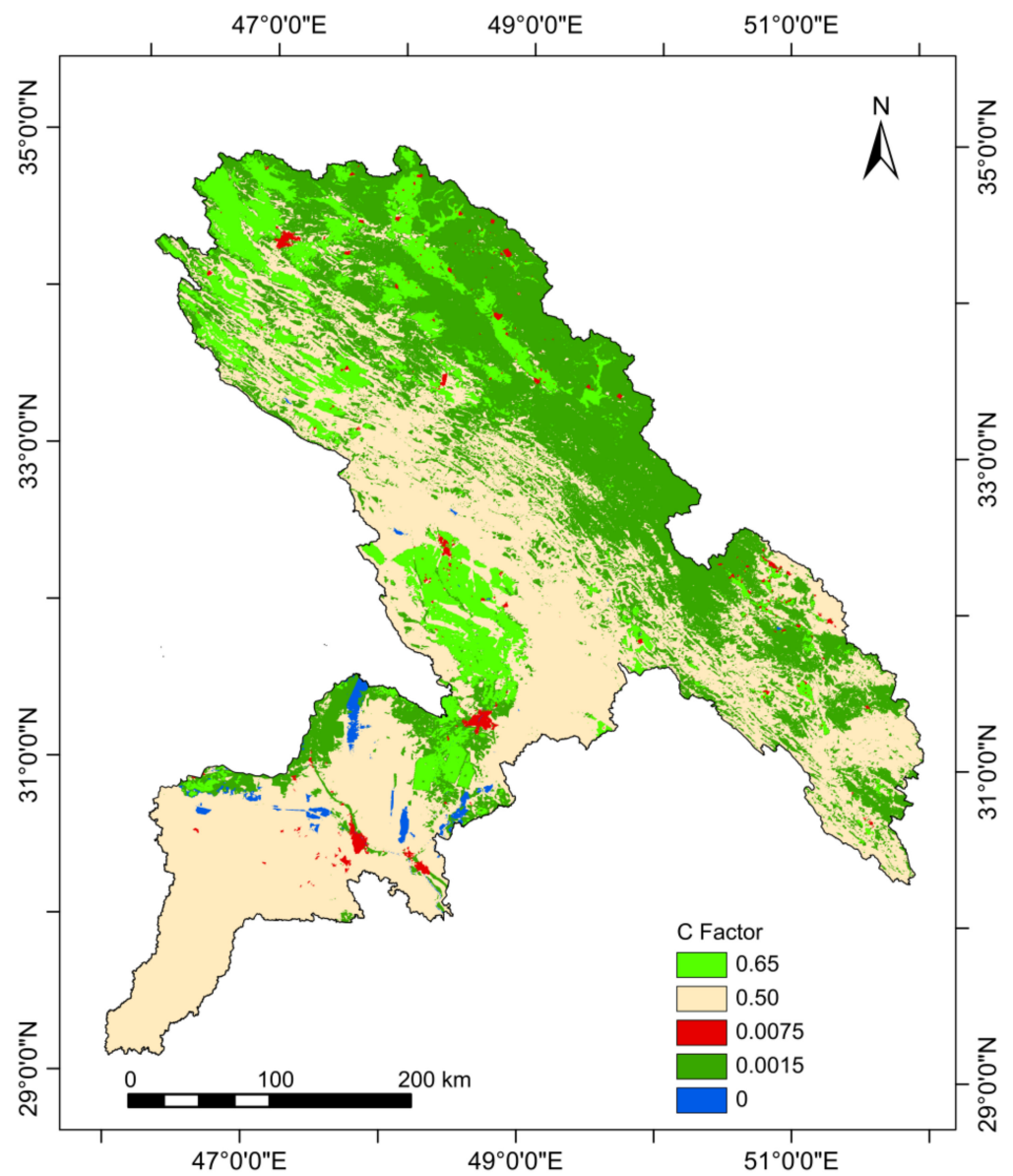


Figure 6. Spatial distribution of C factor in the study area.

4.5. Conservation Support Practice Factor (P Factor)

The P factor is controlled by the terrain slope (Equation (4)). The overall slope pattern in the study area demonstrates the steepest slope in the northern and eastern parts and decreases towards the southwest [61]. Therefore, high P factor values are anticipated in the northern and eastern parts, and low values are in the southwestern parts of the basin (Figure 7). A P factor of 0.20 to 0.54; 0.54 to 1.22; 1.22 to 2.04; 2.04 to 3.33; and 3.33 to 17.56 represents 50.9, 26.9, 15.1, 6.1, and 0.9% of the basin’s area, respectively.

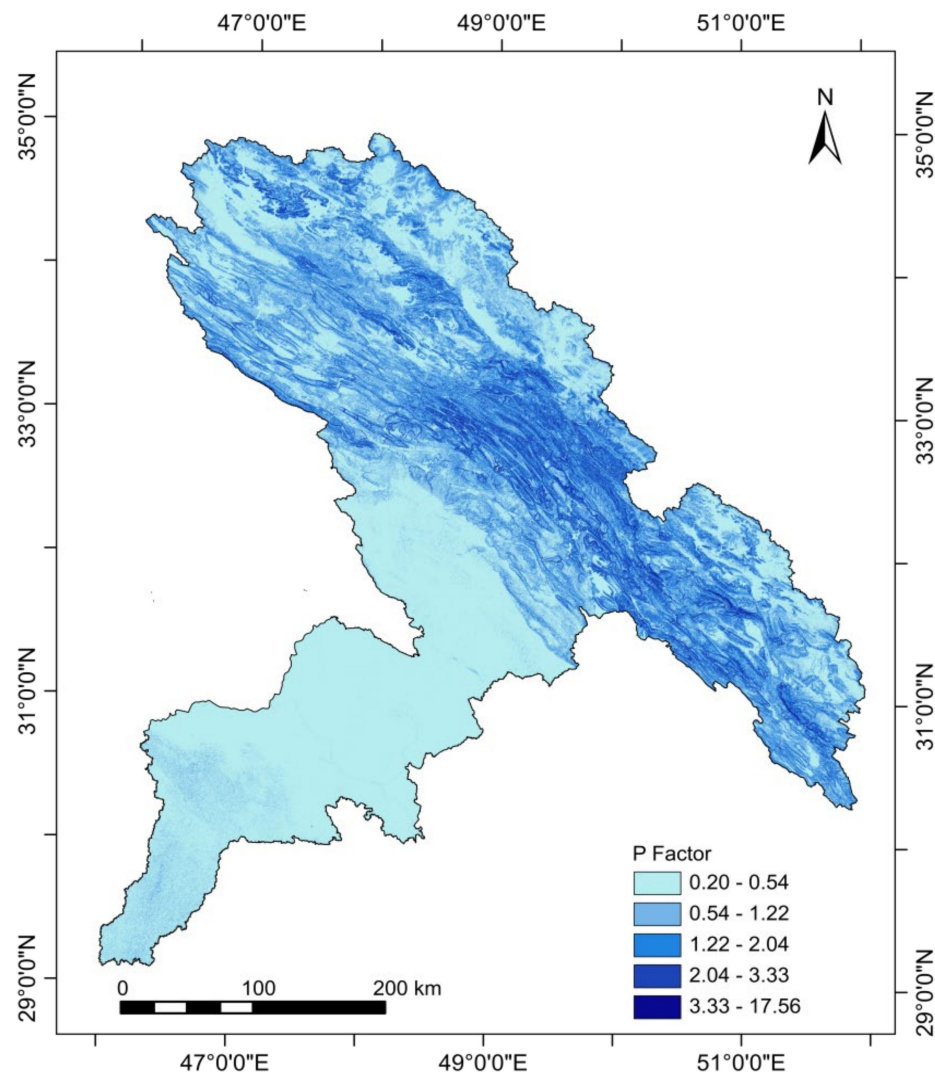


Figure 7. Spatial distribution of P factor in the study area.

4.6. Estimation of Potential Soil Erosion

Rainfall erosivity, slope length and steepness, soil erodibility, land cover management, and soil conservation represent the main erosion contributors. Figures 3–7 illustrate the results of the modeling of these factors. The modeling of rainfall erosivity reveals that the higher the rainfall intensity, the higher its erosion potential. The soil erodibility parameter, which indicates both the soil's vulnerability to erosion and the rate of runoff, demonstrate that the least transport-resistant soils that generate large runoff had the highest values for K parameter. Modeling the slope's length and gradient reveal that the steeper the slope, the larger the runoff velocities and, thus, the greater the erosion. Similarly, slope improves the conservation support practice parameter, and thus erosion. The cover and management component that indicates how various LULC types affect soil loss rates [48] reveal that farmland and bare land have the greatest values, while shrub land and urban land use have the lowest. Although all five RUSLE parameters influence the ultimate soil erosion rate, these parameters have a different impact on the erosion rate in the current study. The analyses in this study reveal that such parameters vary in different magnitude. For example, P-parameter, LS-parameter, C-parameter, K-parameter, and R-parameter vary by a factor of 85, 50, 43, 17, and 3.3, respectively (Figures 3–7), indicating that these parameters affect erosion rates in the same order. As a result of the final soil loss model, Figure 8 shows the annual erosion map of the study area, which helps to identify the areas that are prone to soil erosion. The annual global average erosion rate is 2.2 tons per hectare [93]. The annual

erosion rates in this study in tons per hectare were extremely high (more than 50); very high (50 to 16.5); high (16.5 to 2.2); medium (2.2 to 1); and low (1 to 0), representing 16, 4, 13, 7, and 60 % of the basin area, respectively. The high soil loss rates are linked to areas of high rainfall levels, loamy soil domination, elevated terrains/plateau margins with a steep side slope, and high cultivation activities. Clearly, the upstream parts of the basin represent areas of high soil erosion potential. Thus, the current study's results may aid in decision-making for improved land conservation and soil management. Public agencies should take the necessary measures to mitigate the influence of these influencing parameters.

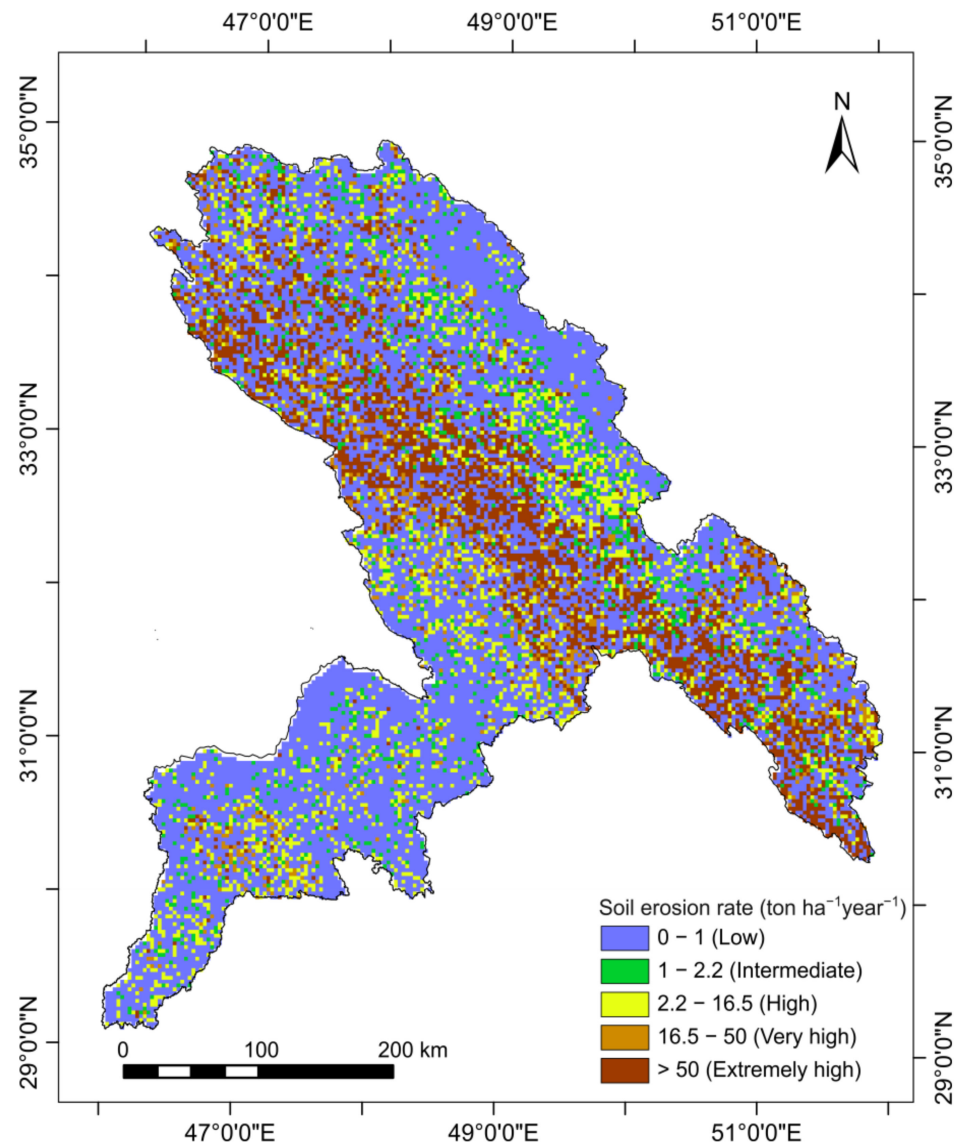


Figure 8. Soil erosion rate distribution in the Shatt Al-Arab basin.

5. Conclusions

This study uses the empirical soil erosion model RUSLE in conjunction with RS and GIS to calculate soil loss rates in the Shatt Al-Arab basin. This soil erosion model was selected because it is straightforward, physically easy to decipher, needs fewer datasets, and can be created using accessible inputs. The RS, GIS, and RUSLE empirical model generated a quantitative assessment of soil losses, which was used to categorize the basin area into six soil erosion risk categories. Extremely high to high soil loss of >50 to 2.2 tons per hectare per year accounts for about 33 percent of the basin's area, while intermediate and low soil loss of less than 2.2 tons per hectare per year comprises the rest of the basin. The erosion

elements affecting soil loss, such as high rainfall levels, loamy soil dominance, elevated terrains/plateau borders with a steep side slope, and high agriculture activities, would promote the high soil loss amount. It was determined that the most severely degraded areas are generally situated in the upstream parts of the investigated basin. In contrast, the slightly deteriorated areas are situated in the watershed's downstream parts. Although the downstream parts of the basin have a limited potential for soil erosion, materials eroded from the upstream parts may collect in the river's lower reaches. This is particularly true for Shatt Al-Arab, where high sedimentation levels in Basra Governorate, situated in the lower reaches of Shatt Al-Arab, recurrently obstruct drainage regimes [14] and, hence, exacerbate floods. Thus, identifying the most influential factors that govern soil erosion is essential to deal with the problem. Positive measures to combat soil erosion can include changing slopes into terraces, improving slope protection, and increasing plant covering. These measures would assist in improving the fragmentation of erosion patches, reducing the erosive force of surface runoff, and reducing the scale impact of erosion. Finally, the results would aid in implementing appropriate erosion preventive actions in badly impacted locations. The study's findings may aid in developing management scenarios and supplying policymakers with solutions for the most efficient policies of soil erosion threats and the prioritizing of basin areas for remediation.

Author Contributions: Conceptualization; methodology; software; formal analysis; investigation; resources; data curation; writing—original draft preparation; visualization; supervision; and project administration, H.A. and C.O. All authors have read and agreed to the published version of the manuscript.

Funding: This research received no external funding.

Institutional Review Board Statement: Not applicable.

Informed Consent Statement: Not applicable.

Data Availability Statement: The authors confirm that the data supporting the findings of this study are available within the article.

Conflicts of Interest: The authors declare no conflict of interest.

References

1. Amundson, R.; Berhe, A.A.; Hopmans, J.W.; Olson, C.; Sztein, A.E.; Sparks, D.L. Soil and human security in the 21st century. *Science* **2015**, *348*, 1261071-1–1261071-6. [CrossRef] [PubMed]
2. Robinson, D.A.; Panagos, P.; Borrelli, P.; Jones, A.; Montanarella, L.; Tye, A.; Obst, C.G. Soil natural capital in Europe; a framework for state and change assessment. *Sci. Rep.* **2017**, *7*, 6706. [CrossRef] [PubMed]
3. Keesstra, S.D.; Bouma, J.; Wallinga, J.; Tiftonell, P.; Smith, P.; Cerdà, A.; Montanarella, L.; Quinton, J.N.; Pachepsky, Y.; van der Putten, W.H.; et al. The significance of soils and soil science towards realization of the United Nations sustainable development goals. *Soil* **2016**, *2*, 111–128. [CrossRef]
4. Borrelli, P.; Robinson, D.A.; Fleischer, L.R.; Lugato, E.; Ballabio, C.; Alewell, C.; Meusburger, K.; Modugno, S.; Schütt, B.; Ferro, V.; et al. An assessment of the global impact of 21st century land use change on soil erosion. *Nat. Commun.* **2017**, *8*, 2013. [CrossRef] [PubMed]
5. Emadodin, I.; Bork, H. Degradation of soils as a result of long-term human-induced transformation of the environment in Iran: An overview. *J. Land Use Sci.* **2012**, *7*, 203–219. [CrossRef]
6. El Jazouli, A.; Ghafiri, A.; El Moutaki, S.; Ettaqy, A.; Khellouk, R. Soil erosion modeled with USLE, GIS, and remote sensing: A case study of Ikkour watershed in Middle Atlas (Morocco). *Geosci. Lett.* **2017**, *4*, 25. [CrossRef]
7. Gayen, A.; Saha, S. Application of weights-of-evidence (WoE) and evidential belief function (EBF) models for the delineation of soil erosion vulnerable zones: A study on Pathro river basin, Jharkhand, India. *Model. Earth Syst. Environ.* **2017**, *3*, 1123–1139. [CrossRef]
8. Sharda, V.; Mandai, D.; Ojasvi, P.R. Identification of soil erosion risk areas for conservation planning in different states of India. *J. Environ. Biol.* **2013**, *34*, 219–226.
9. World Wildlife Fund. Available online: <https://www.worldwildlife.org/threats/soil-erosion-and-degradation#:~:text=The%20effects%20of%20soil%20erosion,water%2C%20which%20can%20worsen%20flooding> (accessed on 1 July 2022).
10. Maina, C.W.; Sang, J.K.; Raude, J.M.; Mutua, B.M.; Moriasi, D.N. Sediment Distribution and Accumulation in Lake Naivasha, Kenya over the Past 50 Years. *Lakes Reserv. Res. Manag.* **2019**, *24*, 162–172. [CrossRef]

11. World Resources Institute. Available online: <https://www.wri.org/insights/causes-and-effects-soil-erosion-and-how-prevent-it> (accessed on 1 July 2022).
12. Gayen, A.; Saha, S.; Pourghasemi, H.R. Soil erosion Assessment using RUSLE model and its Validation by FR probability model. *Geocarto Int.* **2019**, *35*, 1750–1768. [[CrossRef](#)]
13. Comino, J.R.; Keesstra, S.D.; Cerdà, A. Connectivity assessment in Mediterranean vineyards using improved stock unearthing method, LiDAR and soil erosion field surveys. *Earth Surf. Process. Landf.* **2018**, *43*, 2193–2206. [[CrossRef](#)]
14. Ministry of Municipalities and Public Works, Iraq. *Report on Data Collection Survey on Water Sector in Southern Iraq*; Japan International Cooperation Agency NJS Consultants Co., Ltd.: Tokyo, Japan, 2015.
15. Financial Tribune. Available online: <https://financialtribune.com/articles/environment/33787/soil-erosion-in-iran-costs-more-than-oil-revenue> (accessed on 1 July 2022).
16. Earthobservatory.nasa.gov. Floods Ravage Iran and Iraq. Available online: <https://earthobservatory.nasa.gov/images/144785/floods-ravage-iran-and-iraq> (accessed on 1 July 2022).
17. Reliefweb, Iran: Floods Appeal n° MDRIR002 Operation Update #04. Available online: <https://reliefweb.int/report/iran-islamic-republic/iran-floods-appeal-n-mdrir002-operation-update-04> (accessed on 1 July 2022).
18. Reliefweb, Iraq: Flood-Affected Areas in Missan and Basra Governorates as of 18 April 2019. Available online: <https://reliefweb.int/map/iraq/iraq-flood-affected-areas-missan-and-basra-governorates-18-april-2019> (accessed on 1 July 2022).
19. Savari, M.; Gharechae, H. Application of the extended theory of planned behavior to predict Iranian farmers' intention for safe use of chemical fertilizers. *J. Clean. Prod.* **2020**, *263*, 1. [[CrossRef](#)]
20. Koohizadeh, M.; AkhondAli, A.; Arsham, A. The Effect of Soil Moisture Levels on the Threshold Velocity of Wind Erosion in Dust Centers of South and Southeast of Khuzestan Province-Ahwaz. *Iran. J. Soil Water Res.* **2021**, *52*, 869–885. [[CrossRef](#)]
21. Savari, M.; Yazdanpanah, M.; Rouzaneh, D. Factors affecting the implementation of soil conservation practices among Iranian farmers. *Sci. Rep.* **2022**, *12*, 8396. [[CrossRef](#)] [[PubMed](#)]
22. Foroushani, M.A.; Opp, C.; Groll, M. Investigation of Aeolian dust deposition rates in different climate zones of Southwestern Iran. *Atmosphere* **2021**, *12*, 229. [[CrossRef](#)]
23. Foroushani, M.A.; Opp, C.; Groll, M. Spatial and temporal gradients in the rate of dust deposition and aerosol optical thickness in southwestern Iran. *J. Arid. Land* **2021**, *13*, 1–22. [[CrossRef](#)]
24. Bybordi, M. *Soil Physics*; University of Tehran Press: Tehran, Iran, 2003. (In Persian)
25. Emadodin, I.; Narita, D.; Bork, H.R. Soil degradation and agricultural sustainability: An overview from Iran. *Environ. Dev. Sustain.* **2012**, *14*, 611–625. [[CrossRef](#)]
26. Arekhi, S.; Darvishi, A.B.; Shabani, A.; Fathizad, H.; Ahamdyasbchin, S. Mapping Soil Erosion and Sediment Yield Susceptibility using RUSLE, Remote Sensing and GIS (Case study: Cham Gardalan Watershed, Iran). *Adv. Environ. Biol.* **2012**, *6*, 109–124.
27. Fathizad, H.; Karimi, H.; Alibakhshi, S.M. The estimation of erosion and sediment by using the RUSLE model and RS and GIS techniques (Case study: Arid and semi-arid regions of Doviraj, Ilam province, Iran). *Int. J. Agric. Crop Sci.* **2014**, *7*, 304–314.
28. Mesfln, A. The Nile-source of regional cooperation or conflict. In Proceedings of the Eighth Iwra World Congress on Water Resources “Satisfying Future National And Global Water Demand”, Cairo, Egypt, 21–25 November 1994.
29. Renard, K.; Foster, G.R.; Wessies, G.A.; Porter, J.P. RUSLE-Revised universal soil loss equation. *J. Soil Water Conserv.* **1994**, *46*, 30–33.
30. Dutta, D.; Das, S.; Kundu, A.; Taj, A. Soil erosion risk assessment in Sanjal watershed, Jharkhand (India) using geo-informatics, RUSLE model and TRMM data. *Modeling Earth Syst. Environ.* **2015**, *1*, 37. [[CrossRef](#)]
31. Terranova, O.; Antronico, L.; Coscarelli, R.; Iaquinata, P. Soil erosion risk scenarios in the Mediterranean environment using RUSLE and GIS: An application model for Calabria (southern Italy). *Geomorphology* **2009**, *112*, 228–245. [[CrossRef](#)]
32. Jarašiūnas, G.; Šwitoniak, M.; Kinderienė, I. Dynamics of slope processes under changing land use conditions in young morainic landscapes, Western Lithuania. *Int. Agrophys.* **2020**, *34*, 43–55. [[CrossRef](#)]
33. Auerswald, K. Predicted and measured sediment loads of large watersheds in Bavaria. In Proceedings of the Fifth International Symposium on River Sedimentation, Karlsruhe, Germany, 6–10 April 1992; pp. 1031–1036.
34. Auerswald, K. Water erosion. In *The Encyclopedia of Soil Science*; Chesworth, W., Ed.; Springer: Dordrecht, The Netherlands, 2008; pp. 817–822.
35. Poesen, J.; Nachtergaele, J.; Verstraeten, G.; Valentin, C. Gully erosion and environmental change: Importance and research needs. *Catena* **2003**, *50*, 91–133. [[CrossRef](#)]
36. Pan, J.; Wen, Y. Estimation of soil erosion using RUSLE in Caijiamiao watershed. *China Nat. Hazards* **2014**, *71*, 2187–2205. [[CrossRef](#)]
37. Prasannakumar, V.; Shiny, R.; Geetha, N.; Vijith, H. Spatial prediction of soil erosion risk by remote sensing, GIS and RUSLE approach: A case study of Siruvani river watershed in Attapady valley, Kerala, India. *Environ. Earth Sci.* **2011**, *64*, 965–972. [[CrossRef](#)]
38. Boggs, G.; Devonport, C.; Evans, K.; Puig, P. GIS-based rapid assessment of erosion risk in a small catchment in the wet/dry tropics of Australia. *Land Degrad. Dev.* **2001**, *12*, 417–434. [[CrossRef](#)]
39. Lee, S. Soil erosion assessment and its verification using the Universal Soil Loss Equation and Geographic Information System: A case study at Boun, Korea. *Environ. Geol.* **2004**, *45*, 457–465. [[CrossRef](#)]

40. Lu, D.; Li, G.; Valladares, G.S.; Batistella, M. Mapping soil erosion risk in Rondonia, Brazilian Amazonia: Using RUSLE, remote sensing and GIS. *Land Degrad. Dev.* **2004**, *15*, 499–512. [[CrossRef](#)]
41. Lim, K.J.; Sagong, M.; Engel, B.A.; Tang, Z.; Choi, J.; Kim, K.M. GIS-based sediment assessment tool. *Catena* **2005**, *64*, 61–80. [[CrossRef](#)]
42. Bhattarai, R.; Dutta, D. Estimation of soil erosion and sediment yield using GIS at catchment scale. *Water Resour. Manag.* **2007**, *21*, 1635–1647. [[CrossRef](#)]
43. Dabral, P.P.; Baithuri, N.; Pandey, A. Soil erosion assessment in a hilly catchment of North Eastern India using USLE, GIS and remote sensing. *Water Resour. Manag.* **2008**, *22*, 1783–1798. [[CrossRef](#)]
44. Ismail, J.; Ravichandran, S. RUSLE2 model application for soil erosion assessment using remote sensing and GIS. *Water Resour. Manag.* **2008**, *22*, 83–102. [[CrossRef](#)]
45. Tian, Y.C.; Zhou, Y.M.; Wu, B.F.; Zhou, W.F. Risk assessment of water soil erosion in upper basin of Miyun Reservoir, Beijing, China. *Environ. Geol.* **2009**, *57*, 937–942. [[CrossRef](#)]
46. Abdo, H.; Salloum, J. Mapping the soil loss in Marqya basin: Syria using RUSLE model in GIS and RS techniques. *Environ. Earth Sci.* **2017**, *76*, 114. [[CrossRef](#)]
47. Wischmeier, W.H.; Smith, D.D. Prediction Rainfall Erosion Losses from Cropland East of the Rocky Mountains: A Guide for Selection of Practices for Soil and Water Conservation. In *Agricultural Handbook*; U.S. Department of Agriculture: Washington, DC, USA, 1965; No. 282; 47p.
48. Renard, K.G.; Foster, G.R.; Weesies, G.A.; McCool, D.K.; Yoder, D.C. Predicting soil erosion by water: A guide to conservation planning with the revised universal soil loss equation (RUSLE). In *USDA Agricultural Handbook*; U.S. Department of Agriculture: Washington, DC, USA, 1997; No. 703.
49. Millward, A.A.; Mersey, J.E. Adapting the RUSLE to model soil erosion potential in a mountainous tropical watershed. *Catena* **1999**, *38*, 109–129. [[CrossRef](#)]
50. Lin, C.Y.; Lin, W.T.; Chou, W.C. Soil erosion prediction and sediment yield estimation: The Taiwan experience. *Soil Tillage Res.* **2002**, *68*, 143–152. [[CrossRef](#)]
51. Wang, G.; Gertner, G.; Fang, S.; Anderson, A.B. Mapping multiple variables for predicting soil loss by geostatistical methods with TM images and a slope map. *Photogramm. Eng. Remote Sens.* **2003**, *69*, 889–898. [[CrossRef](#)]
52. Jasrotia, A.S.; Singh, R. Modeling runoff and soil erosion in a catchment area, using the GIS, in the Himalayan region, India. *Environ. Geol.* **2006**, *51*, 29–37. [[CrossRef](#)]
53. Bahadur, K. Mapping soil erosion susceptibility using remote sensing and GIS: A case of the Upper Nam Wa Watershed, Nan Province, Thailand. *Environ. Geol.* **2009**, *57*, 695–705. [[CrossRef](#)]
54. Chou, W.C. Modelling watershed scale soil loss prediction and sediment yield estimation. *Water Resour. Manag.* **2010**, *24*, 2075–2090. [[CrossRef](#)]
55. Perovic, V.; Zivotic, L.; Kadovic, R.; Dordevic, A.; Jaramaz, D.; Mrvic, V.; Todorovic, M. Spatial modelling of soil erosion potential in a mountainous watershed of South-eastern Serbia. *Environ. Earth Sci.* **2013**, *68*, 115–128. [[CrossRef](#)]
56. Abedi, M.; Shafizadeh-Moghadam, H.; Morid, S.; Booi, M.J.; Delavar, M. Evaluation of ECMWF mid-range ensemble forecasts of precipitation for the Karun River basin. *Theor. Appl. Climatol.* **2020**, *141*, 61–70. [[CrossRef](#)]
57. Semiromi, F.; Hassani, A.; Torabian, A.; Karbassi, A.R.; Lotfi, F. Evolution of a new surface water quality index for Karoon catchment in Iran. *Water Sci. Technol.* **2011**, *64*, 2483–2491. [[CrossRef](#)] [[PubMed](#)]
58. Marjanizadeh, S. Developing a “Best Case Scenario” for Karkheh River Basin management (2025 horizon); A Case Study from Karkheh River Basin, Iran. Ph.D. Thesis, University of Natural Resources and Applied Life Sciences, Vienna, Austria, 2008.
59. Muthuwatta, L.P.; Ahmad, M.D.; Bos, M.G.; Rientjes, T.H.M. Assessment of Water Availability and Consumption in the Karkheh River Basin, Iran—Using Remote Sensing and Geo-statistics. *Water Resour. Manag.* **2010**, *24*, 459–484. [[CrossRef](#)]
60. Rahimi, N.; Arian, M.; Ghorashi, M. Active Tectonics of the Saymareh-Karkheh River Basin (Northwest of Persian Gulf, Iran). *Open J. Mar. Sci.* **2017**, *7*, 238–257. [[CrossRef](#)]
61. TAVO. *Tübinger Atlas des Vorderen Orients*; Part A IV; Luwig Reichert: Wiesbaden, Germany, 1985.
62. Allafta, H.; Opp, C. GIS-based multi-criteria analysis for flood prone areas mapping in the trans-boundary Shatt Al-Arab basin, Iraq-Iran. *Geomat. Nat. Hazards Risk* **2021**, *12*, 2087–2116. [[CrossRef](#)]
63. Wischmeier, W.H.; Smith, D.D. Predicting rainfall erosion losses. A guide to conservation planning. In *Agriculture Handbook*; US Department of Agriculture: Washington, DC, USA, 1978; Volume 537, p. 85.
64. Prasannakumar, V.; Vijith, H.; Geetha, N.; Shiny, R. Regional Scale Erosion Assessment of a Sub-tropical Highland Segment in the Western Ghats of Kerala, South India. *Water Resour. Manag.* **2011**, *25*, 3715–3727. [[CrossRef](#)]
65. Ganasri, B.P.; Ramesh, H. Assessment of soil erosion by RUSLE model using remote sensing and GIS—A case study of Nethravathi Basin. *Geosci. Front.* **2016**, *7*, 953–961. [[CrossRef](#)]
66. Farhan, Y.; Nawaiseh, S. Spatial assessment of soil erosion risk using RUSLE and GIS techniques. *Environ. Earth Sci.* **2015**, *74*, 4649–4669. [[CrossRef](#)]
67. Amellah, O.; el Morabiti, K. Assessment of soil erosion risk severity using GIS, remote sensing and RUSLE model in Oued Laou Basin (north Morocco). *Soil Sci. Annu.* **2021**, *72*, 142530. [[CrossRef](#)]
68. Thomas, J.; Joseph, S.; Thrivikramji, K.P. Assessment of soil erosion in a tropical mountain river basin of the southern Western Ghats, India using RUSLE and GIS. *Geosci. Front.* **2018**, *9*, 893–906. [[CrossRef](#)]

69. Mohammadi, S.; Karimzadeh, H.; Alizadeh, M. Spatial estimation of soil erosion in Iran using RUSLE model. *EcoHydrology* **2018**, *5*, 551–569. (In Persian)
70. Choudhury, M.K.; Nayak, T. Estimation of soil erosion in Sagar lake catchment of central India. In Proceedings of the International Conference on Water and Environment, Bhopal, India, 15–18 December 2003; pp. 387–392.
71. Parysow, P.; Wang, G.X.; Gertner, G.; Anderson, A.B. Spatial uncertainty analysis for mapping soil erodibility based on joint sequential simulation. *Catena* **2003**, *53*, 65–78. [[CrossRef](#)]
72. FAO Map Catalog. Available online: <http://www.fao.org/geonetwork/srv/en/metadata.showpercent3Fid=14116> (accessed on 1 July 2022).
73. Indian Remote Sensing and GIS: SWAT Soil Data Download. SWAT Soil Data Download. Available online: <http://www.indiaremotensing.com/p/s.html> (accessed on 9 June 2022).
74. Stone, R.P.; Hilborn, D. *Fact Sheet, Universal Soil Loss Equation*; Ministry of Agriculture, Food and Rural Affairs: Guelph, ON, Canada, 2000; p. 12.
75. Liu, B.Y.; Nearing, M.A.; Shi, P.J.; Jia, Z.W. Slope length effects on soil loss for steep slopes. *Soil Sci. Soc. Am. J.* **2000**, *64*, 1759–1763. [[CrossRef](#)]
76. Lastoria, B.; Miserocchi, F.; Lanciani, A.; Monacelli, G. An estimated erosion map for the Aterno-Pescara river Basin. *Eur. Water* **2008**, *21/22*, 29–39.
77. Moore, I.D.; Burch, G.J. Physical basis of the length-slope factor in the universal soil loss equation. *Soil Sci. Soc. Am. J.* **1986**, *50*, 1294–1298. [[CrossRef](#)]
78. Moore, I.D.; Burch, G.J. Modeling Erosion and Deposition. Topographic Effects. *Trans. Am. Soc. Agric. Eng.* **1986**, *29*, 1624–1630. [[CrossRef](#)]
79. Earthdata Search. Available online: <https://search.earthdata.nasa.gov/search> (accessed on 9 June 2022).
80. Fayas, C.M.; Abeysingha, N.S.; Nirmanee, S.K.G.; Samaratinga, D.; Mallawatantri, A. Soil loss estimation using Rusle model to prioritize erosion control in KELANI River Basin in Sir Lanka. *Int. Soil Water Conserv. Res.* **2019**, *7*, 130–137. [[CrossRef](#)]
81. Olika, G.; Iticha, B. Assessment of soil erosion using RUSLE and GIS techniques: A case of Fincha’a Watershed, Western Ethiopia. *Am.-Eurasian J. Agric. Environ. Sci.* **2019**, *19*, 31–36.
82. Yesuph, A.Y.; Dagne, A.B. Soil erosion mapping and severity analysis based on Rusle model and local perception in the Beshillo Catchment of the Blue Nile Basin, Ethiopia. *Environ. Syst. Res.* **2019**, *8*, 17. [[CrossRef](#)]
83. Swarnkar, S.; Malini, A.; Tripathi, S.; Sinha, R. Assessment of uncertainties in soil erosion and sediment yield estimates at ungauged basins: An application to the Garra River basin, India. *Hydrol. Earth Syst. Sci.* **2018**, *22*, 2471–2485. [[CrossRef](#)]
84. United States Geological Survey. EarthExplorer. 2022. Available online: <https://earthexplorer.usgs.gov/> (accessed on 9 June 2022).
85. Enderle, D.; Weih, R. Integrating supervised and unsupervised classification methods to develop a more accurate land cover classification. *J. Ark. Acad. Sci.* **2005**, *59*, 65–73.
86. McPhee, P.J.; Smithen, A.A. Application of the USLE in the Republic of South Africa. *Agric. Eng. S. Afr.* **1984**, *18*, 5–13.
87. Morgan, R.P.C. *Soil Erosion and Conservation*, 2nd ed.; Longman: Essex, UK, 1995; 198p.
88. Shin, G.J. The Analysis of Soil Erosion Analysis in Watershed Using GIS. Ph.D. Thesis, Department of Civil Engineering, Gangwon National University, Gangwon-do, Korea, 1999.
89. Foster, G.R.; Toy, T.J.; Renard, K.G. Comparison of the USLE, RUSLE1.06c, and RUSLE2 for application to highly disturbed lands. In Proceedings of the First Interagency Conference on Research in the Watersheds, Benson, AZ, USA, 27–30 October 2003; pp. 154–160.
90. Lufafa, A.; Tenywa, M.M.; Isabirye, M.; Majaliwa, M.J.G.; Woomer, P.L. Prediction of soil erosion in a Lake Victoria basin catchment using GIS based Universal Soil Loss mode. *Agric. Syst.* **2003**, *76*, 883–894. [[CrossRef](#)]
91. Fu, B.J.; Zhao, W.W.; Chen, L.D.; Zhang, Q.J.; Lü, Y.H.; Gulinck, H.; Poesen, J. Assessment of soil erosion at largewatershed scale using rusle and GIS: A case study in the Loess Plateau of China. *Land Degrad. Dev.* **2005**, *16*, 73–85. [[CrossRef](#)]
92. Institute of Water Research, Michigan State University. Available online: <http://www.iwr.msu.edu/rusle/kfactor.htm#:~:text=RUSLE%20%2D%20an%20online%20soil%20erosion%20assessment%20tool&text=K%20factor%20is%20soil%20erodibility,because%20they%20resistant%20to%20detachment> (accessed on 9 June 2022).
93. Financial Tribune. Available online: <https://financialtribune.com/articles/energy/113053/iran-soil-erosion-7-times-global-average> (accessed on 1 July 2022).